Finite Element-Boundary Element Methods for Dielectric Relaxation Spectroscopy

Stephan C. Kramer and Gert Lube

Abstract We apply the finite element-boundary element method (FEM-BEM) for a smooth approximation of a curvilinear interior interface in a finite domain. This avoids unphysical singularities at the interface due to a piece-wise linear boundary. This type of FEM-BEM coupling arises from simulating the biophysical problem of dielectric relaxation spectroscopy of solvated proteins. Boundary elements convert the linear Poisson problem due to the intramolecular charges of the protein into a boundary condition at the protein-solvent interface. The electro-diffusion of ions in the solvent is modeled as a set of convection-diffusion equations. The spatial distributions of the ion species induce an electrostatic potential which solves a Poisson problem. The gradient of the potential constitutes the convective flow field. The link to experiments is given by computing the stationary ionic current through the system. This requires Robin-type boundary conditions at the electrodes.

1 Introduction

The coupling of finite and boundary element methods, (FEM) and (BEM), is commonly used for interface problems on unbounded domains. Finite elements are applied to bounded "regions of interest" which contain non-linearities, inhomogeneities and other properties which need a well-resolved volume mesh. The BEM part models unboundedness and physical effects described by a homogeneous partial differential equation (PDE) with constant coefficients. In this work we

S.C. Kramer (✉)
Institut für Numerische und Angewandte Mathematik der Universität Göttingen, Lotzestraße 16-18, D-37073 Göttingen, Germany

Max-Planck Institut für biophysikalische Chemie, Am Faßberg 11, D-37077 Göttingen, Germany
e-mail: stkramer@math.uni-goettingen.de; stephan.kramer@mpibpc.mpg.de; sck.goe@googlemail.com

G. Lube
Institut für Numerische und Angewandte Mathematik der Universität Göttingen, Lotzestraße 16-18, D-37073 Göttingen, Germany
e-mail: lube@math.uni-goettingen.de

A. Abdulle et al. (eds.), *Numerical Mathematics and Advanced Applications - ENUMATH 2013*, Lecture Notes in Computational Science and Engineering 103, DOI 10.1007/978-3-319-10705-9_4

discuss how to employ BEM to exclude a subdomain from a finite domain. This accurately models the geometric shape of an interior, curvilinear and smooth interface and unifies the computational domain for the components of a PDE model.

The investigation of this subclass of FEM-BEM coupling arises from the need to simulate the biophysical problem of dielectric relaxation spectroscopy (DRS) of solvated proteins, in particular ubiquitin, which plays a fundamental role in cell biology. The discovery of ubiquitin-mediated protein degradation won the nobel prize in chemistry in 2004. The physical basis of DRS is the polarizability of non-conducting materials in the presence of an external electric field. Polarization is the material-specific part of the dielectric displacement which is proportional to the electric field. The proportionality is given by the complex dielectric permittivity ε^*. In the frequency domain it quantifies the dynamic response of molecular dipoles (contributing at high frequencies) and mobile charge carriers (predominant influence at low frequencies). The DRS technique allows to measure dielectric properties in the range of 10^{-6}–10^{12} Hz. For a detailed review see the monograph [1]. The typical experimental setup is a parallel plate capacitor with the dielectric sample in between the plates [1, Chapter 2]. Application of an alternating voltage yields the dielectric loss spectrum, i.e. the conductivity-corrected imaginary part of ε^* as function of frequency. In case of ubiquitin in aqueous solution this spectrum is dominated by the "γ" peak at about 10 GHz, which represents the reorientation of the dipoles of water molecules in the bulk, and the "β" peak at roughly 10 MHz which accounts for the tumbling motion of the protein molecule while its molecular dipole aligns with the applied electric field [2]. This is sketched in Fig. 1a. The peak positions reveal the time scales on which the relaxation processes take place. Recent DRS studies on ubiquitin [3] suggest that the dynamics of conformational sampling, i.e. a protein's ability to switch between different molecular conformations (indicated by the different positions of the intramolecular charges in Fig. 1b, c), influence the direct current component of the dielectric loss spectrum and can be observed as the "sub-β" peak. This important discovery provides a direct experimental access to the rates of the intramolecular dynamics, which are mostly inaccessible to nuclear magnetic resonance (NMR) spectroscopy, the most frequently used experimental

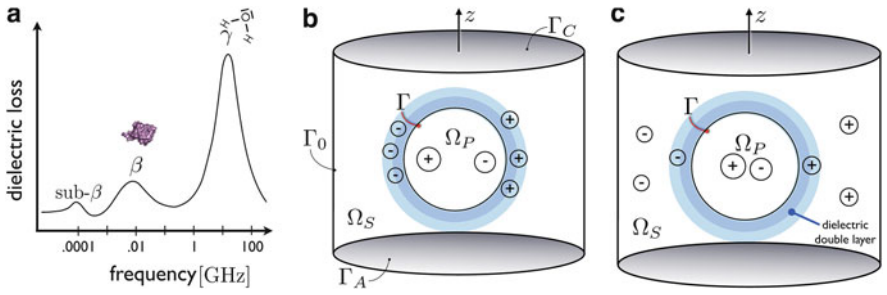

Fig. 1 (**a**) Dielectric loss spectrum of ubiquitin. (**b**, **c**) Charge configurations in protein (domain Ω_P) in the DRS cell $\Omega = \Omega_S \cup \Omega_P$. Details see text

technique to characterize protein dynamics. For the detailed explanation of many biomolecular processes, e.g. of protein-protein recognition [4], the exact knowledge of the kinetics of conformational sampling is decisive.

In this paper we apply the theory of FEM-BEM methods for infinite domains to the case of using the BEM part to exclude a subdomain from a finite domain in order to develop a deeper understanding of the origin of the "sub-β" peak. We use BEM to retain the smooth shape of the protein-solvent interface. The proper incorporation of a stationary current by means of Robin-type boundary conditions (BCs) provides the link to a comparison with experimental data. The equations are solved by the geometric multigrid (GMG) method [5] from deal.II [6].

2 Poisson-Nernst-Planck Model

Initial theoretical studies explained the "sub-β" peak by a 2-state, ratchet-like stochastic model for the conformational dynamics coupled to a Fokker-Planck model for the mobile ions [3, supplementary material]. Depending on its conformation the ubiquitin molecule may bind a varying number of ions in its dielectric double layer thus influencing the density of mobile ions responsible for the direct current component. Although it explains the essential features of the "sub-β" peak, this stochastic model neither includes spatial inhomogeneities nor BCs.

For the effects at the protein-solvent interface Γ we need at least a generic anion and cation species with densities c_- and c_+, respectively, with charges of equal strength. To incorporate a stationary current through the DRS cell (Fig. 1), we have to take into account the redox reaction $\mathrm{I}^+ + \mathrm{e}^- \leftrightarrow \mathrm{N}$ for converting a cation I^+ into a neutral particle N at the cathode Γ_C or the anode Γ_A. Thus, we have to incorporate the density c_0 of the neutral particles. The stochastic description of the ion dynamics is replaced by the Poisson-Nernst-Planck equations

$$\partial_t c_a = -\nabla \cdot \mathbf{j}_a \,, \tag{1a}$$

$$\mathbf{j}_a = -(\nabla c_a + a c_a \nabla \Phi) \tag{1b}$$

$$-\nabla \cdot (\varepsilon_r(\mathbf{r}) \nabla \Phi) = -(c_+ - c_-)\chi_{\Omega_S} + \rho_f \tag{1c}$$

for non-dimensional ion densities $c_a : \Omega_S \to \mathbb{R}$, $a \in \{+, 0, -\}$, electro-diffusive fluxes $\mathbf{j}_a : \Omega_S \to \mathbb{R}^3$ and electrostatic potential $\Phi : \Omega \to \mathbb{R}$. The charge density on the right-hand side of Eq. (1c) comprises the mobile ions in the subdomain of the solvent Ω_S, indicated by its characteristic function χ_{Ω_S}, and the intramolecular, conformation-specific charge distribution ϱ_f, indicated by the index f. Here, the protein is a dipole with two point charges immersed in a spherical, dielectric domain $\Omega_P = \Omega \backslash \Omega_S$, $\Omega_P \cap \Omega_S = \emptyset$. The function ε_r in Eq. (1c) is piece-wise constant and denotes the relative permittivities, i.e. $\varepsilon_r = \varepsilon_S \approx 80$ on Ω_S, $\varepsilon_r = \varepsilon_P \approx 2$ on Ω_P. Note the different computational domains for ions, Ω_S, and potential, Ω.

A realistic description of DRS requires BCs for the $\mathbf{j}_a$ and Φ capable of modeling an applied current. Usually, the redox reaction rates K_R and K_O are described by Butler-Volmer kinetics, including the Frumkin correction due to the Stern layer [7]. As discussed in [8], for Φ Dirichlet BCs, $\Phi\big|_{\Gamma_C} = \Phi_C$, $\Phi\big|_{\Gamma_A} = \Phi_A$, suffice. The redox reaction implies a balance of in- and outward fluxes at the electrodes

$$\mathbf{n}\cdot\mathbf{j}_+\big|_{\Gamma_C} = K_R\, c_+\big|_{\Gamma_C} = \; -\mathbf{n}\cdot\mathbf{j}_0\big|_{\Gamma_C}\,, \tag{2}$$

$$-\mathbf{n}\cdot\mathbf{j}_+\big|_{\Gamma_A} = K_O\, c_0\big|_{\Gamma_A} = \mathbf{n}\cdot\mathbf{j}_0\big|_{\Gamma_A}\,, \tag{3}$$

where $\mathbf{n}$ is the outer normal of the surface $\partial\Omega_S$ and $\cdot|_B$ is the trace on some part $B \subset \partial\Omega_S = \Gamma_C \cup \Gamma_0 \cup \Gamma_A \cup \Gamma$. The rates are treated as constants, especially their dependence on Φ is neglected. The anions do not contribute to the current transport and fulfill $\mathbf{n}\cdot\mathbf{j}_-|_{\Gamma_A} = \mathbf{n}\cdot\mathbf{j}_-|_{\Gamma_C} = 0$. The hull Γ_0 of the cell and the protein surface Γ are impermeable for all ions, $\mathbf{n}\cdot\mathbf{j}_a|_{\Gamma_0} = \mathbf{n}\cdot\mathbf{j}_a|_{\Gamma} = 0$, $a \in \{+,0,-\}$. For Φ we have $\mathbf{n}\cdot\nabla\Phi|_{\Gamma_0} = 0$ and Γ is a dielectric interface with continuity and the jump relations

$$\lim_{\delta\to 0}\Phi(\mathbf{x}-\delta\mathbf{n}) = \lim_{\delta\to 0}\Phi(\mathbf{x}+\delta\mathbf{n})\,, \qquad \varepsilon_P(\mathbf{x})\mathbf{n}\cdot\nabla\Phi = \varepsilon_S(\mathbf{x})\mathbf{n}\cdot\nabla\Phi \quad \forall\mathbf{x}\in\Gamma \tag{4}$$

One goal in computational biochemistry is to model molecular surfaces of proteins in a smooth manner [9]. Instead of an accurate sub-cell resolution of the dielectric interface Γ we convert the interior constant-coefficient-Poisson equation into a boundary integral equation (BIE) on Γ. The protein becomes an excluded volume Ω_P of constant dielectric permittivity $\varepsilon_r = \varepsilon_P$ containing point charges $\{q_k\}$ at fixed positions $\{\mathbf{x}_k\}$. To do this, we apply the discussion of the BIE formulation for linear interior Neumann boundary value and interface problems in [10]. The Johnson-Nédélec coupling [11] needs the normal component of the electric field w.r.t. to the outer normal $\mathbf{n}_P$ ($\mathbf{n}_P = -\mathbf{n}$ on Γ) of Ω_P as independent variable $t^P := -\partial_{\mathbf{n}}\Phi$. Potential theory shows that on C^1-smooth, closed surfaces Γ the intramolecular part Φ_P of the potential at $\mathbf{x}\in\Gamma$ fulfills

$$\frac{1}{2}\Phi(\mathbf{x}) + \oint_\Gamma\left[\Phi(\mathbf{x}')\frac{\partial G_{\mathbf{x}}}{\partial\mathbf{n}'_P}(\mathbf{x}') - G_{\mathbf{x}}(\mathbf{x}')\frac{\partial\Phi}{\partial\mathbf{n}'_P}(\mathbf{x}')\right]d\Gamma(\mathbf{x}') = \frac{1}{\varepsilon_P}\int_{\Omega_P} G_{\mathbf{x}}(\mathbf{x}')\rho_f(\mathbf{x}')\,.$$

Here, $G_{\mathbf{x}}(\mathbf{y}) := 1/(4\pi|\mathbf{x}-\mathbf{y}|)$ is the Green's function of the Laplace equation. The right-hand side defines the Newton potential ϕ^C. We define the single layer boundary integral operator (BIO) $V : H^{-1/2}(\Gamma) \to H^{1/2}(\Gamma)$ and the double layer BIO $K : H^{1/2}(\Gamma) \to H^{1/2}(\Gamma)$ as in [12, Secs. 6.2 and 6.4]. Instead of $\mathbf{n}_P$ we use the outward normal $\mathbf{n} = -\mathbf{n}_P$ relative to Ω_S

$$(Vt^P)(\mathbf{x}) := \oint_\Gamma G_{\mathbf{x}}(\mathbf{x}')t^P(\mathbf{x}')d\Gamma(\mathbf{x}')\,, \qquad (K\Phi_P)(\mathbf{x}) := \oint_\Gamma \frac{\partial G_{\mathbf{x}}}{\partial\mathbf{n}(\mathbf{x}')}(\mathbf{x}')\Phi(\mathbf{x}')d\Gamma(\mathbf{x}')\,.$$

From Eq. (4) follows $\varepsilon_S \partial_{\mathbf{n}} \Phi\big|_{\Gamma} = -\varepsilon_P t^P$ and we get

$$\left(\frac{1}{2} I - K\right) \Phi + \frac{\varepsilon_S}{\varepsilon_P} V t^P = \phi^C \,. \tag{5}$$

This is the basis for the FEM-BEM method for the potential, reducing its computational domain to $\Omega_S = \Omega \backslash \Omega_P$. The distribution of the ions is governed by convection-diffusion equations with either Neumann or Robin but no Dirichlet BCs. The link to experiments is the direct current I_{dc} created by a potential difference $\eta := \Phi_C - \Phi_A$. Due to the redox reaction at the electrodes $I_{dc} = \int_{\Gamma_C} \mathbf{n} \cdot \mathbf{j}_+ d\Gamma_C = K_R \int_{\Gamma_C} c_+ d\Gamma_C$. The conformational sampling introduces a time-dependence on I_{dc}. This is modeled by a two-state telegraph process, i.e. a random switching between two stationary states. This makes Eq. (1a) formally time independent. For details cf. [8]. To validate the hypothesis about the origin of the "sub-β" peak we have to compute two different values for I_{dc} from the time independent version of Eq. (1).

3 Weak Formulation and Discretization

We do not solve Eq. (1) in its mixed form, but reduce it to a set of convection-diffusion equations by inserting Eq. (1b) into Eq. (1a), eliminating the currents.

Let $(\cdot,\cdot)_D$ be the L^2 inner product on a domain D and $\|\cdot\|_X$ the norm of a function space X. For $D \equiv \Omega_S$ we drop the index. The weak form of Eq. (1) is derived by multiplying with test functions, integrating by parts and inserting all flux BCs. The Dirichlet BCs for the potential Φ are built into the solution space X for the FEM part. We define X as a direct product of a space $X^c := [H^1(\Omega_S)]^3$ for the densities and $X^\Phi := \{\Phi \in H^1(\Omega_S) : \Phi|_{\Gamma_A} = 0,\ \Phi|_{\Gamma_C} = \eta\}$ for Φ. For the BCs for Φ on Γ we need the space $Y := H^{-1/2}(\Gamma)$. The final solution space is $V := X \times Y$. The FEM part of the solution is $\mathbf{u} := (c_+, c_0, c_-, \Phi)$ and the test function is $\mathbf{v} := (s, u, v, w)$. Except for the interface term for Φ on Γ the weak form is a semilinear form $a(\cdot;\cdot) : X \times X \to \mathbb{R}$ which is nonlinear in its first argument. The terms in $a(\cdot;\cdot)$ can be grouped to reflect, after linearizing, the block structure of the matrix using scalar test functions as block row and trial functions as block column indexes. Diagonal terms are in $a_D(\cdot;\cdot)$, linear upper off-diagonal terms in $a_U^l(\cdot;\cdot)$, nonlinear drift terms in $a_U^d(\cdot;\cdot)$ and lower off-diagonal terms in $a_L(\cdot;\cdot)$, i.e.

$$\begin{aligned}
a_D(\mathbf{u};\mathbf{v}) &:= (\nabla s, \nabla c_+) + (\nabla u, \nabla c_0) + k_O (u, c_0)_{\Gamma_A} + (\nabla v, \nabla c_-) + \varepsilon_S (\nabla w, \nabla \Phi), \\
a_U^l(\mathbf{u};\mathbf{v}) &:= -k_O (s, c_0)_{\Gamma_A}\,, \quad a_U^d(\mathbf{u};\mathbf{v}) := (\nabla s, c_+ \nabla \Phi) - (\nabla v, c_- \nabla \Phi)\,, \\
a_L(\mathbf{u},\mathbf{v}) &:= -k_R (u, c_+)_{\Gamma_C} - (w, c_+ - c_-)\,.
\end{aligned}$$

After linearizing $a_U^d(\cdot;\cdot)$ w.r.t. c_+ and c_-, the associated matrices are A_D, A_U and A_L, respectively. The left-hand side of the weak form of Eq. (5), with associated matrices B_K and B_V, is a sum of the two bilinear forms

$$\begin{aligned} b_K(\psi,\Phi) &:= \left(\psi, \left(\tfrac{1}{2}I - K\right)\Phi\right)_\Gamma &&: H^{1/2}(\Gamma)\times H^{1/2}(\Gamma)\to\mathbb{R}\,, \\ b_V(\psi,t^P) &:= \tfrac{\varepsilon_S}{\varepsilon_P}\left(\psi, Vt^P\right)_\Gamma &&: H^{-1/2}(\Gamma)\times H^{1/2}(\Gamma)\to\mathbb{R}\,. \end{aligned}$$

We use conformal discretizations $X_h \subset X$ and $Y_h \subset Y$ by globally continuous Lagrange elements for which we use deal.II's `FE_Q<dim>` class. In practice, the trial functions in Y_h are given by the traces of those in X_h because we treat the normal derivative as independent variable. This is due to the way finite elements are implemented in deal.II. The same holds for the test functions ψ in the dual space $Y_h' \subset H^{1/2}(\Gamma)$. Then, the discretized variational problem is: *Find* $(\mathbf{u}_h, t_h^P) \in X_h \times Y_h$ *s. t.*

$$\forall \mathbf{v}_h \in X_h \;:\quad a(\mathbf{u}_h;\mathbf{v}_h) + (w, \varepsilon_P t^P)_\Gamma \;=\; 0\,, \tag{6a}$$

$$\forall \psi_h \in Y_h' \;:\quad b_K(\psi_h,\Phi_h) + b_V(\psi_h, t_h^P) = \left(\psi_h, \phi^C\right)_\Gamma\,. \tag{6b}$$

Several numerical problems arise in solving the discretized problem. Only the potential Φ is unambiguous since it is subject to Dirichlet BCs at the electrodes Γ_A and Γ_C. The equation for the density of the neutral particles c_0 effectively is a pure Neumann Laplace problem. Its average merely enters via the boundary terms in Eq. (3) for the cations c_+. Particle numbers, and thus average densities, are conserved $\int_{\Omega_S} c_a \, d\Omega_S = const$, $a \in \{+,0,-\}$ in the stationary state. This is enforced by adding a pseudo-time dependence, i.e. $-\nabla^2 u = f$ becomes $[\delta I - \nabla^2]u^{n+1} = f + \delta u^n$, where δ is an inverse time step and I is the identity operator.

We solve by interleaving successive mesh refinement, pseudo-time stepping and reassembly of the nonlinear terms. This introduces a sequence of finite-dimensional subspaces $X_h \subset X$, parametrized by the cell diameter h. On a given mesh, i.e. in FE space $V_h^\ell \subset V$, $V_h^\ell \subset V_h^{\ell+1}$ we run a few steps in pseudo-time (while $\|u^{n+1} - u^n\|_{\ell_2} \geq Tol$). In each time step we reassemble the drift terms in A_U after solving the linear algebraic problem by deal.II's GMRES solver with left-preconditioning.

For the numerical solution of Eq. (6) we have considerably extended the GMG example step-16 of deal.II, v7.2.0. When computing the matrices B_K, B_V from the bilinear forms $b_K(.,.)$ and $b_V(.,.)$ the double integration is avoided by using the support points of the test functions for collocation. With $t_h^P = \sum_i t_i^P \phi_i \in Y_h$, e.g. the entries of the matrix representing the single layer BIO are formally given by $B_{V,ij} = (\psi_i, V\phi_j)$. Let $\mathbf{x}_i$ be the support point of DoF i, then collocation at $\mathbf{x}_i$ can be interpreted as $B_{V,ij} = (\delta(\mathbf{x}-\mathbf{x}_i), V\phi_j)$, i.e. $B_{V,ij}$ is computed as

$$B_{V,ij} = \oint_{\partial\Omega_S} G_{\mathbf{x}_i}(\mathbf{x}')\phi_j(\mathbf{x}')d\Gamma(\mathbf{x}')\,. \tag{7}$$

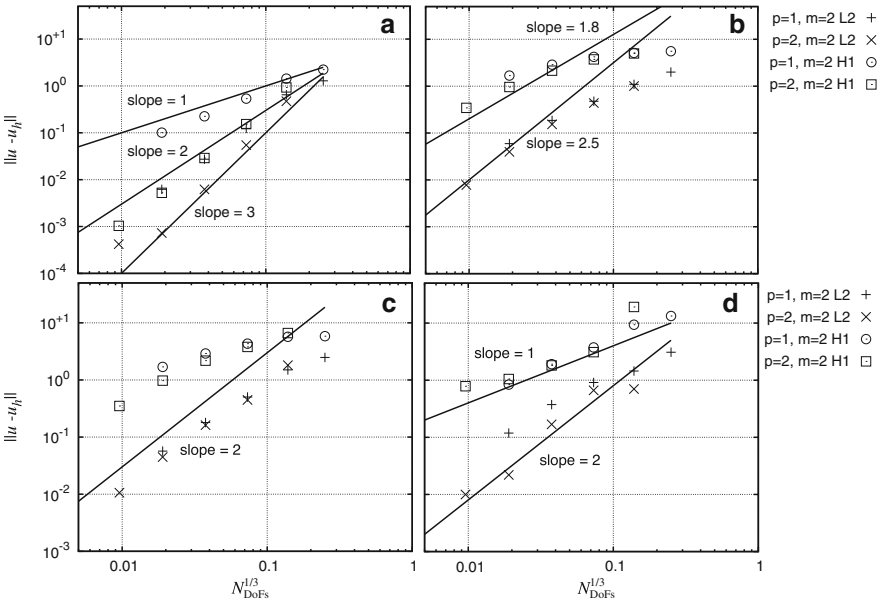

Fig. 2 Convergence of the Neumann problem, Eq. (11), with (**a**) Eq. (8), (**b**) Eq. (9) as solution. (**c**) FEM and (**d**) BEM error for dipole test case, Eq. (9), on the FEM-BEM problem, Eq. (10). Figures share axis labels and legends

To minimize the costs of matrix assembly we compute bulk and boundary mass matrices only once. The definitions of X^c and X^Φ require the assembly of two different Laplacians and hence to setup two GMG preconditioners P_{MG}^c and P_{MG}^Φ. Cell contributions get reused when building global matrices which differ only in the BCs. The costs of assembling the matrices by numerical quadrature are roughly equal to two Poisson equations with variable coefficients as the data for the linear Laplacians can be reused to a great extent for the drift terms. The matrix A for the linearized DRS problem, Eq. (6), is stored as `dealii::BlockMatrixArray` and the preconditioner P_A as `dealii::BlockTrianglePecondition` which acts like a block Gauss-Seidel method. Its diagonal blocks are $(P_{MG}^c, P_{MG}^c, P_{MG}^c, P_{MG}^\Phi, P^V)$, where P^V preconditions B_V and is the identity matrix. The upper off-diagonal blocks of P_A are void. The lower off-diagonal blocks are those of A, i.e. A_L and B_K.

Results and Conclusion

In our tests we model the boundary piece-wise by polynomials of order $m = 2$, cf. legend of Fig. 2. This numerical boundary is not C^1-smooth. According to our tests, it approximates the curved surface of a sphere sufficiently well such that we do not have to consider the solid angle subtended by the surface

(continued)

elements at a vertex of the mesh of Γ. Due to the outer surface of the DRS cell we cannot use the C^1-mapping provided by deal.II as deal.II cannot assign different mappings to different subboundaries. Throughout we use either linear ($p = 1$) or quadratic ($p = 2$) FEM.

We are interested in the convergence of our method for the pure Neumann problem and for the FEM-BEM coupling. We define two test problems with solutions

$$\Phi_{SP} := 0.1(2x + y + z) + 0.01xyz\,, \tag{8}$$

$$\Phi_D := \frac{1}{4\pi|\mathbf{x} - \mathbf{x}_+|} - \frac{1}{4\pi|\mathbf{x} - \mathbf{x}_-|}\,, \tag{9}$$

with $\mathbf{x}_\pm = (0, 0, \pm 0.5)$ in a sphere of radius 1. As Φ_{ref} is either Φ_{SP} or $\Phi_{DSP} := \Phi_D + \Phi_{SP}$. Note that Φ_{SP} is harmonic. The FEM-BEM convergence is assessed on the simplified problem: *find* $(\Phi, t^P) \in X^\Phi \times Y$ *s.t.* $\forall (v, \psi) \in X^\Phi \times Y'$:

$$(\nabla v, \varepsilon_S \nabla \Phi) + (v, \varepsilon_S t^P)_\Gamma = 0\,, \tag{10a}$$

$$b_K(\psi_h, \Phi_h) + b_V(\psi_h, t_h^P) = \left(\psi, \phi^C\right)_\Gamma\,, \tag{10b}$$

with $\Phi|_{\Gamma_A \cup \Gamma_0 \cup \Gamma_C} = \Phi_{ref}$. The test for pure Neumann BCs is: *find* $\Phi \in H^1(\Omega_S)$ *s.t.*

$$(\nabla v, \nabla \Phi) = (v, \partial_{\mathbf{n}} \Phi_{ref}) \quad \forall v \in H^1(\Omega_S)\,. \tag{11}$$

To measure the error we use the standard $L^2(\Omega_S)$- and $H^1(\Omega_S)$-norm for the FEM part. For the BEM part we measure the L^2 error of the trace of Φ on Γ $\|\Phi_{ref} - \Phi_h\|^2_{L^2(\Gamma)}$, and the L^2 error in the trace of $\partial_n \Phi \equiv -t^P$ on Γ. Here, denoted as $H^1(\Gamma)$ semi-norm $|\Phi_{ref} - \Phi_h|^2_{H^1(\Gamma)} := \|\partial_n \Phi_{ref} + t_h^P\|^2_{L^2(\Gamma)}$. In case of Eq. (11) and $\Phi_{ref} = \Phi_{SP}$ convergence is as expected. For FEM of order p we get $\|u - u_h\|^2_{L^2(\Omega_S)} = O(h^{p+1})$ and $\|u - u_h\|^2_{H^1(\Omega_S)} = O(h^p)$ independent of the order of the boundary approximation m, cf. Fig. 2a. Figure 2b shows that for $\Phi_{ref} = \Phi_{DSP}$ we roughly lose half an order which we attribute to the right-hand side of the BEM part containing the δ-distributions for the point charges. Figure 2c shows the convergence of the FEM part of Eq. (10). For Lagrange finite elements of order $p = 2$ the $L^2(\Omega_S)$ and $H^1(\Omega_S)$ error have the same asymptotic behavior. The error in the BEM part, Fig. 2d, is as expected for linear elements ($p = 1$). Due to the collocation the decay of the error in t^P does not improve. The error of $\Phi|_\Gamma$ partly profits from higher order elements. Figure 3 shows that local inhomogeneities of the cation density in

(continued)

the vicinity of the protein surface are resolved and the current-carrying species (cations and neutral particles) are distributed opposite to each other.

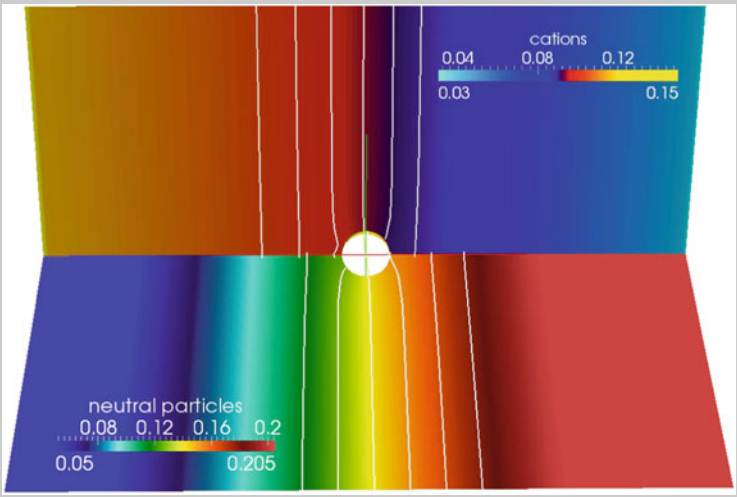

Fig. 3 Distribution of cations and neutral particles in the DRS cell

To conclude, we have derived a mathematical model for the detailed simulation of the electro-diffusive processes in dielectric relaxation spectroscopy of proteins in solution including boundary effects inaccessible in previously derived stochastic models. The key feature is the modeling of the protein-solvent interface as excluded volume with a smooth surface by taking into account its electrostatic properties by means of a boundary integral equation. For the efficient solution of the resulting FEM-BEM model we have extended the geometric multigrid example of the deal.II library (step-16) to vector-valued problems and higher order elements. Unlike the strategy proposed in deal.II's step-34 for boundary elements we have to use the traces of the finite elements as boundary elements. Most of the equations in the DRS model are pure Neumann problems and subject to a conservation of particle numbers. To assure their unique solvability we implemented an interleaved pseudo-time stepping/mesh refinement strategy which avoids the saddle-point problems arising from Lagrange multipliers. The convergence is as expected. The convergence of the FEM-BEM method depends on the particular test case but is consistent with the literature. Applied to the full DRS problem our numerical results indicate the validity of the proposed explanation of the origin of the "sub-β" peak.

References

1. F. Kremer, A. Schönhals, *Broadband Dielectric Spectroscopy* (Springer, Berlin/New York, 2003)
2. A. Knocks, H. Weingärtner, The dielectric spectrum of ubiquitin in aqueous solution. J. Phys. Chem. B **105**(17), 3635–3638 (2001)
3. D. Ban et al., Kinetics of conformational sampling in ubiquitin. Angew. Chem. Int. Ed. **50**(48), 11437–11440 (2011)
4. C. Kleanthous, *Protein-Protein Recognition* (Oxford University Press, Oxford/New York, 2000)
5. B. Janssen, G. Kanschat, Adaptive multilevel methods with local smoothing for H^1- and H^{curl}-conforming high order finite element methods. SIAM J. Sci. Comput. **33**(4), 2095–2114 (2011)
6. W. Bangerth, R. Hartmann, G. Kanschat, deal.II – a general purpose object oriented finite element library. ACM Trans. Math. Softw. **33**(4), 24/1–24/27 (2007)
7. W. Schmickler, E. Santos, *Interfacial Electrochemistry* (Springer, New York, 2010)
8. S.C. Kramer, Cuda-based scientific computing – tools and selected applications, Ph.D. thesis, Georg-August Universität Göttingen, 2012
9. C.L. Bajaj, G. Xu, Q. Zhang, A fast variational method for the construction of resolution adaptive C^2-smooth molecular surfaces. Comput. Methods Appl. Mech. Eng. **198**(21), 1684–1690 (2009)
10. S. Rjasanow, O. Steinbach, *The Fast Solution of Boundary Integral Equations* (Springer, New York/London, 2007)
11. C. Johnson, J. Nédélec, On the coupling of boundary integral and finite element methods. Math. Comput. **35**(152), 1063–1079 (1980)
12. O. Steinbach, *Numerical Approximation Methods for Elliptic Boundary Value Problems*. Texts in Applied Mathematics (Springer, New York/London, 2007)